Colloids and Surfaces B: Biointerfaces 123 (2014) 710–715

Contents lists available at ScienceDirect

Colloids and Surfaces B: Biointerfaces

journal homepage: www.elsevier.com/locate/colsurfb

Needle-free transdermal delivery using PLGA nanoparticles: Effect of particle size, injection pressure and syringe orifice diameter

Chan Hee Park[a], Leonard D. Tijing[b], Cheol Sang Kim[a], Kang-Min Lee[c,*]

[a] Division of Mechanical Design Engineering, Chonbuk National University, Jeonju 561-756, Republic of Korea
[b] School of Civil and Environmental Engineering, University of Technology, Sydney (UTS), P.O. Box 123, 15 Broadway, NSW 2007, Australia
[c] Department of Molecular Biology, College of Natural Science, Chonbuk National University, Jeonju 561-756, Republic of Korea

ARTICLE INFO

Article history:
Received 3 July 2014
Received in revised form
25 September 2014
Accepted 5 October 2014
Available online 12 October 2014

Keywords:
Skin penetration
Nanoparticles
Needle-free injector
Transdermal
Polyacrylamide gel

ABSTRACT

The aim of this study is to investigate the effects of particle size and other injection factors on the skin penetration of nanoparticles delivered with a needle-free injector. Experimental and simulation tests were carried out at various parameters. In addition to testing different sizes of nanoparticles, we also observed the effects of several injection pressures and syringe orifice diameters (SOD) on the dispersion pattern of the nanoparticles after injection. Our results showed that as the nanoparticle size increased from 45 nm to 452 nm, the resulting puncture opening, channel diameter, and depth of the nanoparticle dispersion decreased, but the width of the dispersion increased. Conversely, as the SOD increased, the puncture opening, channel diameter, and depth of the dispersion increased, but width of the dispersion decreased. Increasing the injection pressure also decreased the size, depth, and width of the puncture opening. These results identify how these three parameters affect nanoparticle delivery from a needle-free injector; therefore, our findings will be beneficial for optimization and further study of needle-free injectors as a mechanism for transdermal delivery of nanoparticles.

1. Introduction

Skin is by far the largest and most easily accessible organ in the human body, and several studies have reviewed topical and systemic delivery of drugs via transdermal methods [1–6]. Transdermal drug delivery provides many therapeutic and practical advantages, including sustained local delivery of drugs, which could reduce systemic side effects; and lighter dosing schedules (meaning fewer doses to achieve the same effect), which might improve patient compliance. Perhaps most importantly, transdermal delivered compounds avoids the first-pass metabolism effect, an advantage that is especially applicable to compounds with poor oral bio-availability [2,7,8].

Although transdermal delivery has been demonstrated as a promising drug delivery mechanism, the functional properties of skin that make it an excellent barrier also limit the efficiency of drug delivery into and across the epidermis [2,5,9]. The skin represents an extraordinary evolutionary feat. It basically consists of three layers, an epidermis composed of columnar epithelium, a dermis composed of fibrous connective tissue, and a hypodermis. The stratum corneum, the uppermost layer of the skin, is relatively impermeable, which makes the transdermal transport of molecules a slow process [10–13]. To overcome the barrier function of the stratum corneum, substances are routinely delivered using a needle. A needle-free alternative jet injection of substances has recently emerged as a novel tool for transdermal drug delivery. The jet injection penetrates the skin and delivers the substance using a high-speed stream of fluid, thus mediating needle-free transdermal drug administration [14–16].

The efficiency of jet penetration into human skin depends on various parameters, according to recent reports [14,16], and dispersion of jets into human and animal skin has been reported for isolated conditions only [17]. Although jet injectors have been thoroughly investigated in clinical trials and animal experiments, the current body of literature contains very little mechanistic evidence underlying the physical events that occur during the injection process [17,18].

Additionally, in recent years, scientists have devoted significant resources toward developing nanotechnology as a tool for drug delivery [19]. Colloidal carriers, such as polymeric nanoparticles, have been investigated as a tool for localized drug delivery to specific anatomical sites, e.g., the eye [20], nose [21,22], brain [23], or intestine [24]. Polymeric nanoparticles have demonstrated several advantages in these studies, such as excellent tolerability, physical

* Corresponding author. Tel.: +82 63 270 3342; fax: +82 63 270 3345.
E-mail address: kmlee@jbnu.ac.kr (K.-M. Lee).

http://dx.doi.org/10.1016/j.colsurfb.2014.10.009
0927-7765/

stability, and protection of labile substances, high drug payload, and the possibility for controlled drug release [16,25], all of which might improve the overall efficiency of the transdermal drug delivery process. Therefore, nanoparticles lend themselves to needle-free injection, because using both technologies simultaneously might bring about a synergistic boost in the efficiency of the transdermal drug delivery.

The idea is promising, but to date there has not been a rigorous study characterizing the parameters that affect the dispersion of nanoparticles during needle-free injection, information that is essential to evaluating the efficiency of the technique. Herein, we demonstrate that the efficiency of jet penetration/dispersion of nanoparticles is dependent on several parameters, namely particle size, injection pressure, and the diameter of the syringe nozzle.

2. Materials and methods

2.1. Materials

Didodecyldimethylammonium bromide (DMAB) and propylene carbonate (PC) were purchased from Sigma (St. Louis, MO, USA). The type of poly-D,L-lactic-co-glycolic acid (PLGA) used herein was obtained from Boehringer Ingelheim (Ingelheim, Germany). All other chemicals were of HPLC grade and purchased from Sigma (St. Louis, MO, USA).

2.2. Nanoparticle preparation

The PLGA nanoparticles were prepared using the emulsification–diffusion method. Briefly, 10–50 mg of PLGA was dissolved in 1 ml of polycarbonate. The resulting organic phases were combined with 2 ml of an aqueous phase containing DMAB (0.1–3%) as stabilizer. After mutual saturation of the organic and aqueous phases, the mixture was emulsified for 1 min in an ice-bath using either a homogenizer or a probe-tip sonicator (Sonicator® XL, Misonix, Farmingdale, NY, USA) at 50 W. In order to mediate the diffusion of the organic solvent into the water, a constant volume (8 ml) of water was subsequently added to the organic/water (o/w) emulsion under moderate magnetic stirring, which led to the formation of PLGA nanoparticles.

2.3. Particle size measurement

Particle size and polydispersity index were determined by the light scattering method, following the manufacturer's recommendations (DLS-8000, Otsuka Electronics, Japan). To conduct measurements, 0.2 ml of the nanoparticle suspension was dispersed in 3 ml of distilled water. The analyses were performed at a scattering angle of 90° and temperature of 25 °C. Each sample was measured in triplicate, and average particle sizes were expressed as mean diameters.

2.4. Preparation of mouse skin

Hairless mice (SKH-hr-1 strain), about 7–8 weeks old, were sacrificed using spinal cord dislocation, and the abdominal skin was wiped clean with a tissue moistened with normal saline. Rectangular sections of whole skin, several centimeters in length and width, were excised with surgical scissors. Following removal of fat and subdermal tissues, the sections were frozen at −70 °C for one week until use.

2.5. Polyacrylamide gels

Polyacrylamide gels (25% acrylamide) were used as a model soft material in this study. The gel were created by adding a polymerization initiator (10% ammonium persulfate, APS) and propagator (N,N,N′,N′-tetramethylethylenediamine, TEMED) to a 50% (w/v) acrylamide solution of 49:1 acrylamide to bis-acrylamide. Specifically, this acrylamide solution was prepared by mixing 10 ml of the 50% stock acrylamide solution with 10 ml of distilled water, and it was polymerized with 200 μl of 10% APS and 40 μl of TEMED.

Table 1
Components of the nanoparticle formulation, and influence of concentration of PLGA, DMAB and energy source on nanoparticle size.

	Nanoparticle			
	I	II	III	IV
PLGA	2%	3%	2%	2%
DMAB	3%	0.3%	3%	0.3%
Emulsion energy	Sonication	Sonication	Homogenization	Stirring

2.6. Experimental transdermal delivery system and simulation analysis

A commercial needle-free injector (Biojector 2000; Portland, OR, USA) was used to produce jets through three different syringe orifice diameters (SOD; 0.114 mm, 0.218 mm, and 0.373 mm) at pressures ranging between 500 psi and 700 psi. Immediately prior to jet injection experiments, the excised mouse skin was mounted onto a polyacrylamide gel base (both described above). Utilizing the needle-free injector, we subjected the nanoparticle solution described above to this experimental transdermal delivery model, as follows: using a spray driven by compressed carbon dioxide (CO_2) gas, nanoparticles were propelled through the mouse skin into the polyacrylamide gel [26]. Specifically, 0.1 mL of nanoparticle solution was loaded into the device, and a jet produced at various pressure and syringe orifice diameter (SOD) settings drove the solution through the mouse skin and into the gel. For performance analysis after injection, the channel diameter, the puncture opening diameter, and the width and depth of the nanoparticle dispersion in the gel were measured using a caliper.

The simulation on pressure and velocity distribution measurement of a commercial needle-free injector configurations was carried out using COMSOL® Ver.4.3 add-on CFD module under Windows Vista operational system. Simulation was performed using the actual configuration of needle-free injector.

3. Results and discussion

3.1. Preparation and characterization of four different size ranges of nanoparticles

Herein, we studied how transdermal dispersion of a nanoparticle solution using a jet injector at a constant jet volume (0.1 ml) was affected by a range of SOD (0.114–0.373 mm), pressures (500–700 psi), and nanoparticle size ranges (45–450 nm). The different sizes of PLGA nanoparticles were prepared using the emulsification–diffusion method; to confirm and optimize nanoparticle formation, we analyzed the particle size in the resulting solution by light scattering. Using various concentrations of DMAB and devices that produced different emulsion intensities (a homogenizer versus a sonicator), we created four different nanoparticle size ranges, which we designated as NP I, II, II and IV (Fig. 1) (Table 1). Our light scattering analyses revealed that the average NP sizes of NP I, II, III, and IV were 45.0 ± 2.3 nm, 82.3 ± 7.2 nm, 222.6 ± 12.3 nm, and 452.2 ± 20.2 nm, respectively. We used these four populations of nanoparticles to study the effects of particle size on dispersion following injection.

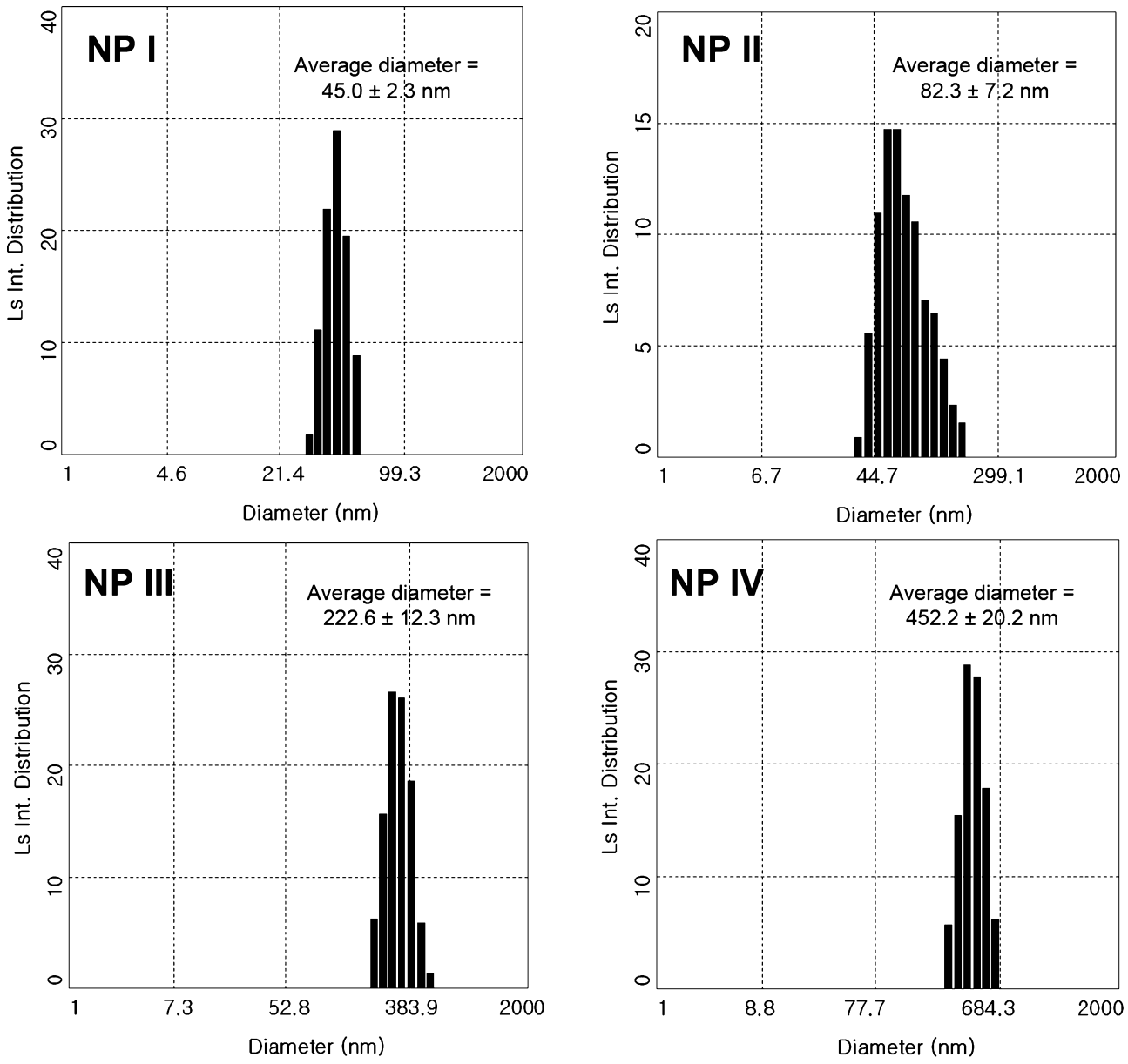

Fig. 1. Size distribution of polymeric nanoparticles: NPI, NPII, NPIII and NPIV at different concentrations of PLGA and DMAB, and at various energy sources.

3.2. Transdermal delivery system using hairless mouse skin and polyacrylamide gel experimental model

The distance of jet penetration into intact skin is limited in part by the composite structure of the skin and by variability in the mechanical properties within and between skin samples [27]. Furthermore, skin is opaque, making it impossible to visualize the extent of transdermal jet dispersion. To overcome these problems, we utilized harvested mouse skin placed onto a polyacrylamide gel bed as our transdermal delivery model.

Polyacrylamide gels have been used as a model test bed for several fluid impingement applications [18,28,29], and they meet several criteria for a model soft material (transparency, controllable mechanical properties, and controllable dimensions). Additionally, the typical jet penetration and dispersion pattern into a polyacryamide gel bed has been described previously: a cylindrical introductory channel followed by a large circular dispersion [18]. This pattern reflects the nature of jet injection of a liquid (whether into skin or polyacrylamide gel), which occurs in two sequential steps. In the first step, the injectate penetrates the skin, fat, and muscle tissue while traveling at a high velocity. The channel results from gel erosion due to the impact of the high-velocity jet. In the second step, the bulk of the injectate is deposited within the target tissue at a lower velocity [30], resulting in a circular dispersion. Although the dispersion pattern seen in polyacrylamide gels does not exactly recapitulate the pattern in skin and tissue, due to differences in material properties, we expect that the needle-free injection parameters tested herein would affect the dispersion pattern in skin and tissue in a similar fashion.

A typical penetration and dispersion pattern created by jet penetration into a 25% polyacrylamide gel is shown in Fig. 2 (82.3 ± 7.2 nm nanoparticles, 0.114 mm SOD, 700 psi pressure, and 0.1 ml jet volume, injected through hairless mouse skin). Jet injection of the nanoparticle solution formed a slender, cylindrical channel originating at the point of impact. The cylindrical channel terminated into a large circular dispersion region, into which the

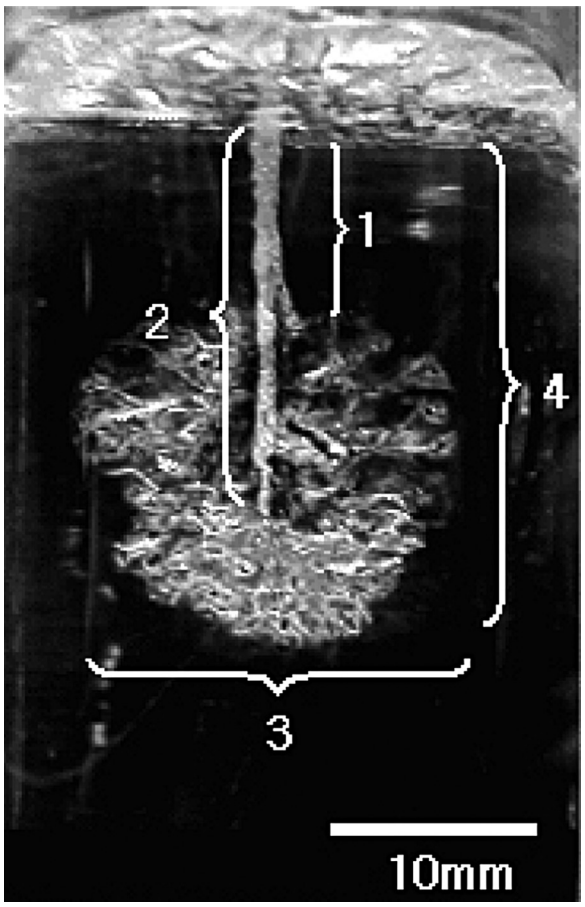

Fig. 2. The general shape of the penetration into the gel (1: channel, 2: hole, 3: width, 4: depth).

majority of the injected liquid was delivered. This pattern recapitulated previous observations of jet injection into a polyacrylamide gel bed.

3.3. Effect of nanoparticle size on dispersion width and injection depth

Using this model system, we first investigated how the penetration of the biojector depended on the size of the nanoparticles in the injection solution. For each experiment, we ejected a total of 0.1 mL of the nanoparticle solution from a biojector fitted with a 0.218-mm diameter. Results were displayed as measurements in each dimension for the set of injections performed with each particle size (Fig. 3). As the particle size increased from 45 nm to 452 nm, the puncture opening decreased from 11.2 mm to 6.1 mm, the channel diameter increased from 5.6 mm to 6.5 mm, the dispersion depth decreased from 23.6 mm to 18.1 mm, and the dispersion width increased from 17.2 mm to 20.8 mm. In other words, as the particle size increased, the general injection depth was decreased, possibly due to the interaction between larger particles on the mouse skin structure. Specifically, we propose that increased friction between the skin structure and the larger particles could decrease the velocity of the injection.

3.4. Effect of SOD on jet penetration

Next, we investigated how the SOD affected jet penetration. For each experiment, a total of 0.1 mL of nanoparticle solution was ejected through varying SOD at a constant pressure (600 psi). Our results revealed that the size of the injector orifice diameter

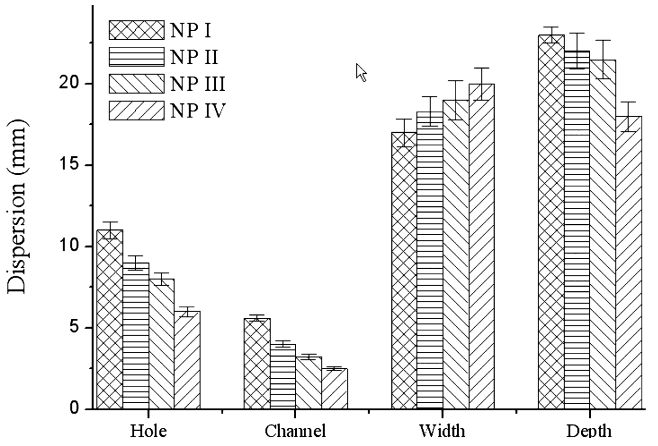

Fig. 3. Characteristics of jet penetration after injection of nanoparticles into acryamide gel through hairless mouse skin and then stomach muscle with respect to particle size (gel concentration 25%, pressure 500 psi).

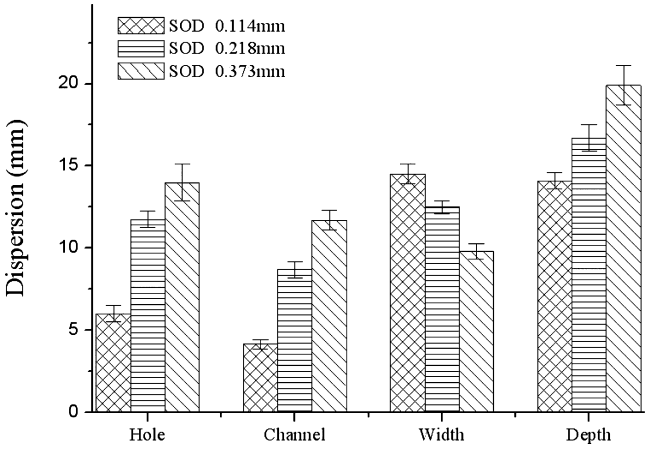

Fig. 4. Characteristics of jet penetration after injection of nanoparticles into acryamide gel through hairless mouse skin with respect to syringe orifice diameter (gel concentration 25%, injection pressure 500 psi).

influenced the shape and dispersion pattern (Fig. 4). As the SOD increased from 0.114 mm to 0.373 mm, the puncture opening in the gel increased from 6.2 mm to 14.0 mm, the channel diameter increased from 4.5 mm to 11.7 mm, the dispersion depth increased from 14.1 mm to 19.9 mm, and the dispersion width decreased from

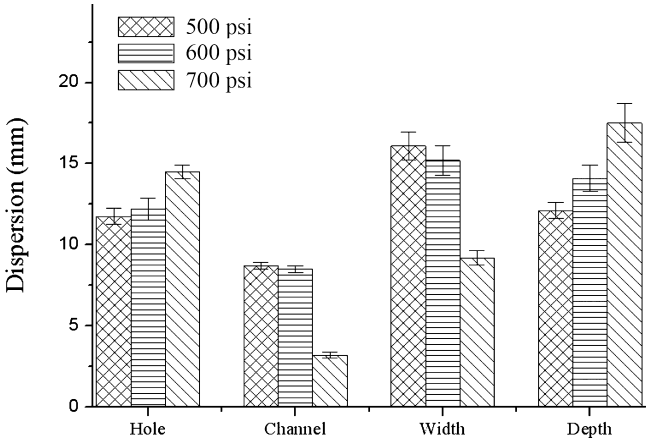

Fig. 5. Characteristics of jet penetration after injection of nanoparticles into acryamide gel through hairless mouse skin with respect to injection pressure (gel concentration 25%, SOD 0.218 mm).

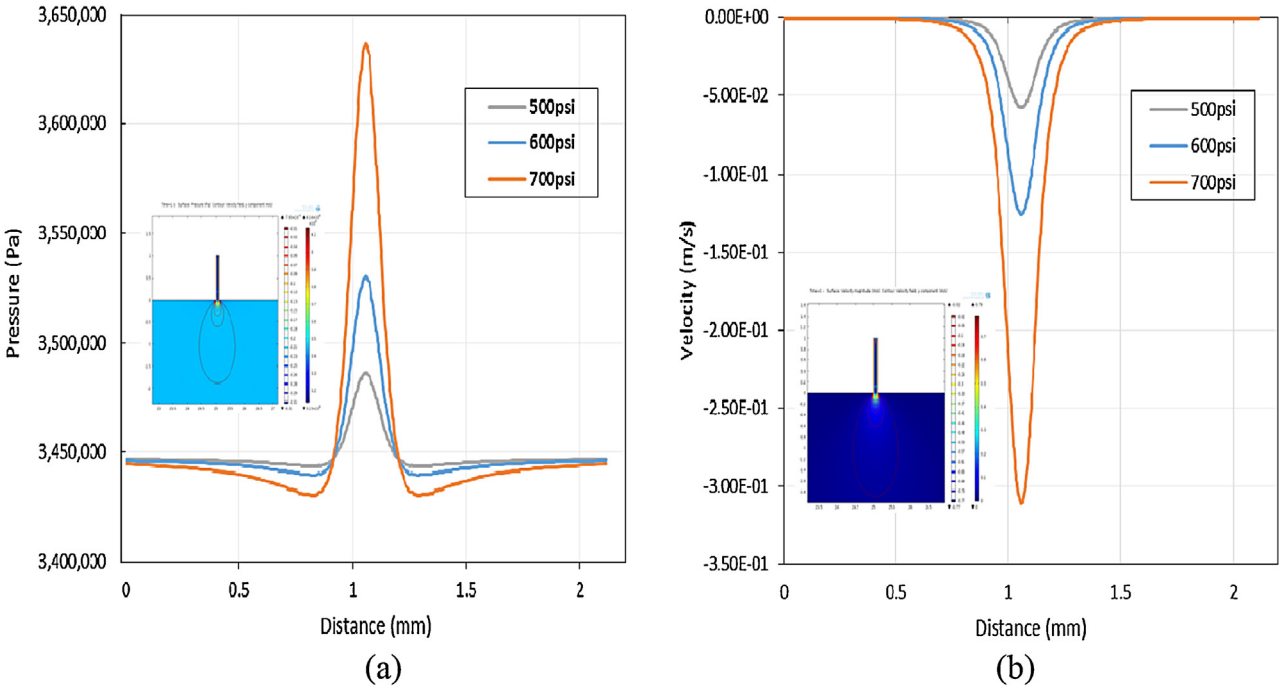

Fig. 6. FEM analysis results showing amplitude of pressure (a) and velocity (b) at different configurations; rainbow scale view (insets).

14.5 mm to 9.8 mm. The shape of the dispersion also changed as the SOD increased, varying from an inverted hemisphere at 0.114 mm SOD, to an ellipsoid at 0.218 mm SOD (the manufactured SOD), to a vertical, more linear shape at 0.373 mm (data not shown). We attributed these observations to the variable flow properties through the different SOD. The flow of the nanoparticle solution through a smaller orifice could have caused both turbulent and frictional losses in the energy of the particle dispersion, if the SOD was a limiting factor in overall jet velocity. Thus, as the jet diameter increased, the rate of energy transfer through the skin also increased, thereby leading to a possible increase in delivery.

3.5. *Effect of pressure on dispersion and penetration of nanoparticles*

To investigate the dependence of nanoparticle penetration on pressure, we utilized the biojector with the manufactured SOD of 0.218 mm and varied the pressure of the CO_2 gas driving the injection. Specifically, we set the device at the selected values of 500, 600 and 700 psi and examined the resulting nanoparticle dispersion patterns (Fig. 5). As the pressure increased from 500 psi to 700 psi, the puncture opening and dispersion depth both increased, but the channel diameter and dispersion width both decreased. The experimental results are in cohesion with the computer simulation output results (Fig. 6). When we increased the pressure from 500 psi to 700 psi, the values of velocity and pressure were also increased under same conditions of polyacrylamide gels.

The effect of increasing the pressure from 600 psi to 700 psi was especially pronounced: the channel diameter and width of the dispersion significantly decreased, from 8.5 mm to 3.2 mm and from 15.2 mm to 9.2 mm, respectively. The nanoparticle solution could not penetrate the mouse skin under a 500-psi injection pressure. Fig. 7 shows a typical cross-sectional image of the penetration pattern of nanoparticle solutions with different nanoparticle sizes onto a porcine tissue.

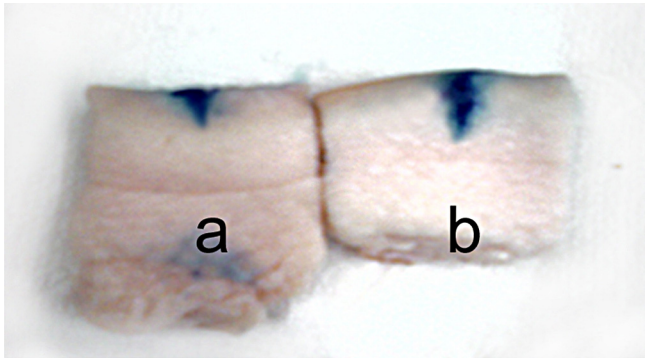

Fig. 7. Cross-sectional views of porcine tissue after bioject injection with nanoparticle size of (a) 45 nm, and (b) 450 nm (syringe orifice diameter of 0.114 mm, pressure of 600 psi, injection volume of 0.1 ml).

4. Conclusion

We prepared four size ranges (45–450 nm) of nanoparticles by varying the polymer concentration, the emulsifying method, and the energy source for emulsion during preparation. Using these nanoparticles and a commercially available needle-free injector, we investigated the influence of different injection parameters on the resulting nanoparticle dispersion pattern through hairless mouse skin into a polyacrylamide gel bed. Our results revealed that during needle-free injection of nanoparticles, both the penetration and the dispersion patterns of the nanoparticles were influenced by all three parameters tested herein: SOD, injection pressure, and the size of the injected particles. As we increased SOD and pressure, the puncture opening in the skin, depth of dispersion penetration, and channel diameter increased, but width of dispersion decreased. However, as we increased the particle size in the injectate, the puncture opening, channel diameter, and dispersion depth decreased, while the dispersion width increased. Increases in injection pressure were accompanied by decreases in the channel diameter and the dispersion width. Significantly, when using needle-free injection to deliver therapeutic substances, the depth of a jet injection and the nature of the dispersion pattern all have the potential to influence the efficacy of drug delivery. These provide

significant information that will aid in the study of transdermal delivery using needle-free injectors and nanoparticles.

Acknowledgements

This research was supported by grant from the Basic Science Research Program through the National Research Foundation of Korea (NRF) under the Ministry of Education, Science and Technology (Project no. 2013R1A2A2A04015484).

References

[1] S. Indermun, R. Luttge, Y.E. Choonara, P. Kumar, L.C. du Toit, G. Modi, V. Pillay, Current advances in the fabrication of microneedles for transdermal delivery, J. Control. Release 185 (2014) 130–138.
[2] A. Alexander, S. Dwivedi, T.K. Ajazuddin, S. Giri, S. Saraf, D.K. Saraf, Tripathi, Approaches for breaking the barriers of drug permeation through transdermal drug delivery, J. Control. Release 164 (2012) 26–40.
[3] T.W. Prow, J.E. Grice, L.L. Lin, R. Faye, M. Butler, W. Becker, E.M.T. Wurm, C. Yoong, T.A. Robertson, H.P. Soyer, M.S. Roberts, Nanoparticles and microparticles for skin drug delivery, Adv. Drug Deliv. Rev. 63 (2011) 470–491.
[4] S.E. Cross, M.S. Roberts, Physical enhancement of transdermal drug application: is delivery technology keeping up with pharmaceutical development, Curr. Drug. Deliv. 1 (2004) 81–92.
[5] B.J. Thomas, B.C. Finnin, The transdermal revolution, Drug Discov. Today 9 (2004) 697–703.
[6] Y.K. Demir, Z. Akan, O. Kerimoglu, Characterization of polymeric microneedle arrays for transdermal drug delivery, PLOS ONE 8 (2013) e77289.
[7] R.L. Bronaugh, R.F. Stewart, J.E. Storm, Extent of cutaneous metabolism during percutaneous absorption of xenobiotics, Toxicol. Appl. Pharmacol. 99 (1989) 534–543.
[8] L. Margetts, R. Sawyer, Transdermal drug delivery: principles and opioid therapy, Continuing Education in Anaesthesia, Crit. Care Pain 7 (2007) 171–176.
[9] B.W. Barry, Novel mechanisms and devices to enable successful transdermal drug delivery, Eur. J. Pharm. Sci. 14 (2001) 101–114.
[10] H. Imoto, Z. Zhou, A.L. Stinchcomb, G.L. Flynn, Transdermal prodrug concepts: permeation of buprenorphine and its alkyl esters through hairless mouse skin and influence of vehicles, Biol. Pharm. Bull. 19 (1996) 263–267.
[11] D.-D. Kim, Y.W. Chien, Transdermal delivery of zalcitabine: in vitro skin permeation study, AIDS 9 (1995) 1331–1336.
[12] T. Nishimura, M. Akimoto, M. Miyazaki, M. Nomoto, M. Miyakawa, Developments of transdermal transport system during skin iontophoresis and electroporation, PIERS Online 6 (2010) 759–763.
[13] Y.K. Demir, Z. Akan, O. Kerimoglu, Sodium alginate microneedle arrays mediate the transdermal delivery of bovine serum albumin, PLOS ONE 8 (2013) e63819.
[14] J. Schramm, S. Mitragotri, Transdermal drug delivery by jet injectors: energetics of jet formation and penetration, Pharm. Res. 19 (2002) 1673–1679.
[15] S. Mitragotri, Current status and future prospects of needle-free liquid jet injectors, Nat. Rev. Drug Discov. 5 (2006) 543–548.
[16] Y. Michinaka, S. Mitragotri, Delivery of polymeric particles into skin using needle-free liquid jet injectors, J. Control. Release 153 (2011) 249–254.
[17] J. Schramm-Baxter, S. Mitragotri, Needle-free jet injections: dependence of jet penetration and dispersion in the skin on jet power, J. Control. Release 97 (2004) 527–535.
[18] J. Schramm-Baxter, J. Katrencik, S. Mitragotri, Jet injection into polyacrylamide gels: investigation of jet injection mechanics, J. Biomech. 37 (2004) 1181–1188.
[19] A. Kumari, S.K. Yadav, S.C. Yadav, Biodegradable polymeric nanoparticles based drug delivery systems, Colloids Surf. B: Biointerfaces 75 (2010) 1–18.
[20] R. Cavalli, M.R. Gasco, P. Chetoni, S. Burgalassi, M.F. Saettone, Solid lipid nanoparticles (SLN) as ocular delivery system for tobramycin, Int. J. Pharm. 238 (2002) 241–245.
[21] R. Fernández-Urrusuno, P. Calvo, C. Remuñán-López, J. Vila-Jato, M. José Alonso, Enhancement of nasal absorption of insulin using chitosan nanoparticles, Pharm. Res. 16 (1999) 1576–1581.
[22] R. Ghirardelli, F. Bonasoro, C. Porta, D. Cremaschi, Identification of particular epithelial areas and cells that transport polypeptide-coated nanoparticles in the nasal respiratory mucosa of the rabbit, Biochim. Biophys. Acta (BBA) – Biomembr. 1416 (1999) 39–47.
[23] P. Ramge, R.E. Unger, J.B. Oltrogge, D. Zenker, D. Begley, J. Kreuter, H. Von Briesen, Polysorbate-80 coating enhances uptake of polybutylcyanoacrylate (PBCA)-nanoparticles by human and bovine primary brain capillary endothelial cells, Eur. J. Neurosci. 12 (2000) 1931–1940.
[24] Y. Pan, Y.-J. Li, H.-Y. Zhao, J.-M. Zheng, H. Xu, G. Wei, J.-S. Hao, F.-D. Cui, Bioadhesive polysaccharide in protein delivery system: chitosan nanoparticles improve the intestinal absorption of insulin in vivo, Int. J. Pharm. 249 (2002) 139–147.
[25] S. Moein Moghimi, A. Christy Hunter, J. Clifford Murray, Long-circulating and target-specific nanoparticles: theory to practice, Pharmacol. Res. 53 (2001) 283–318.
[26] Z. Cui, L. Baizer, R.J. Mumper, Intradermal immunization with novel plasmid DNA-coated nanoparticles via a needle-free injection device, J. Biotechnol. 102 (2003) 105–115.
[27] J.C. Stachowiak, T.H. Li, A. Arora, S. Mitragotri, D.A. Fletcher, Dynamic control of needle-free jet injection, J. Control. Release 135 (2009) 104–112.
[28] E.A. Brujan, K. Nahen, P. Schmidt, A. Vogel, Dynamics of laser-induced caviation bubble near elastic boundaries; influence of the elastic modulus, J. Fluid Mech. 433 (2001) 283–314.
[29] D.A. Fletcher, D.V. Palanker, P. Huie, J. Miller, M.F. Marmor, M.S. Blumenkranz, Intravascular drug delivery with a pulsed liquid microjet, Arch. Ophthalmol. 120 (2002) 1206–1208.
[30] O.A. Shergold, N.A. Fleck, T.S. King, The penetration of a soft solid by a liquid jet, with application to the administration of a needle-free injection, J. Biomech. 39 (2006) 2593–2602.